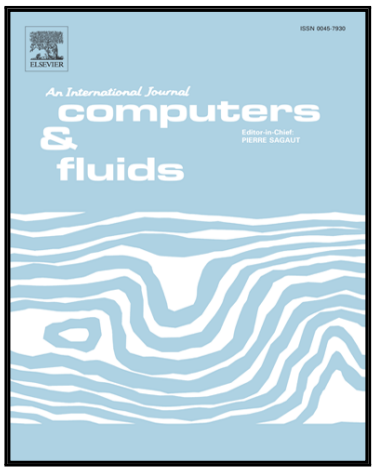

A Direct Numerical Simulation analysis of pressure variation in turbulent premixed Bunsen burner flames-Part 2: Surface Density Function transport statistics

M. Klein , D. Alwazzan , N. Chakraborty

PII: S0045-7930(18)30112-9
DOI: 10.1016/j.compfluid.2018.03.013
Reference: CAF 3774

To appear in: *Computers and Fluids*

Received date: 13 September 2017
Revised date: 13 February 2018
Accepted date: 1 March 2018

Please cite this article as: M. Klein , D. Alwazzan , N. Chakraborty , A Direct Numerical Simulation analysis of pressure variation in turbulent premixed Bunsen burner flames-Part 2: Surface Density Function transport statistics, *Computers and Fluids* (2018), doi: 10.1016/j.compfluid.2018.03.013

Highlights

- Surface Density Function transport analysed for DNS of turbulent Bunsen flames
- Effects of pressure and Reynolds number variations analysed using DNS data
- Effective normal strain rate remains insensitive to the pressure variation
- DL instability at high pressure affects tangential strain and curvature stretch
- Mean contributions of curvature stretch and tangential strain counter each other

A Direct Numerical Simulation analysis of pressure variation in turbulent premixed Bunsen burner flames-Part 2: Surface Density Function transport statistics

M. Klein[a*], D. Alwazzan[b], N. Chakraborty[b]

[a]Universität der Bundeswehr München, Fakultät für Luft- und Raumfahrtechnik, 85577 Neubiberg

[b]School of Mechanical & Systems Engineering, Newcastle University, Newcastle-Upon-Tyne, NE17RU

Abstract

The effects of pressure variation on the transport statistics of the magnitude of the reaction progress gradient (i.e. Surface Density Function (SDF)) have been investigated based on three-dimensional simple chemistry Direct Numerical Simulations (DNS) of Bunsen burner flames representing the flamelet regime of combustion. The large length scale separation between the nozzle diameter and flame thickness for high pressure flames makes the Darrieus-Landau (DL) instability highly likely, which in turn affects the curvature stretch. It has been found that the effective normal strain rate remains insensitive to the pressure variation for the parameter range considered here, which makes the flamelet thickness in turbulent flames comparable to the laminar flame thickness. The influences of the DL instability on the positive mean tangential strain rate counter the effects of instability on the negative mean curvature stretch and thus the effective tangential strain rate (or net flame stretch rate) remains mostly unaffected by the pressure variation within the strict flamelet regime (i.e. wrinkled flamelets and corrugated flamelets regimes) of combustion. The similarities in the SDF and the effective strain rate statistics for different values of pressure suggest that the models for the Flame Surface Density and Scalar Dissipation Rate, which were originally proposed and validated for atmospheric combustion, might remain valid also for elevated pressures.

Keywords:

Premixed flame, Bunsen burner flame, Pressure, Direct Numerical Simulation

* Corresponding Author
Email address: markus.klein@unibw.de

1. INTRODUCTION

The magnitude of the reaction progress variable gradient $|\nabla\tilde{c}|$, which is often referred to as the Surface Density Function (SDF) [1], is a quantity of pivotal importance in turbulent premixed combustion analysis. The transport characteristics of SDF have been utilised for the analysis of pocket formation by Kollmann and Chen [1]. The SDF transport is also important from the point of view of the Flame Surface Density (FSD) [2] and Scalar Dissipation Rate (SDR) [3] transports because of the close relations between the SDF $|\nabla\tilde{c}|$ [2], the generalised FSD $\overline{\rho}\Sigma_{gen}$ [2] and SDR $\widetilde{N}_c = D_c|\nabla\tilde{c}|^2$ [3] where the overbar refers to either Reynolds Averaging or LES filtering, and D_c is the progress variable diffusivity. The influences of turbulence intensity, mean flame curvature, global Lewis number have been analysed by Chakraborty and co-workers [4-6] using simple chemistry DNS data for a canonical configuration representing decaying turbulence in a box. The SDF transport characteristics in methane-air and hydrogen-air flames have been compared by Chakraborty *et al.* [7] using two-dimensional detailed chemistry DNS data. Sankaran *et al*. [8] analysed the SDF statistics from the point of view of characterising the flamelet thickness using three-dimensional detailed chemistry DNS data for Bunsen burner flames. The alignment statistics of $\nabla\tilde{c}$ with local principal strain rates in premixed turbulent flames have been investigated in Refs. [9-12], which revealed that $\nabla\tilde{c}$ aligns with the most extensive principal strain rate when the strain rate induced by flame normal acceleration dominates over turbulent straining and *vice versa*. Recently, Dopazo and co-workers [13-17] linked the evolution of the normal distance between two adjacent reaction progress variable $\tilde{c}$-isosurfaces with the SDF transport equation [4-8] and demonstrated the influences of normal and tangential strain rates arising from flame propagation on the SDF transport. Wang *et al.* [18] and Chaudhury *et al.* [19] analysed $|\nabla\tilde{c}|$ statistics for high-Karlovitz number jet flames and temporally-evolving slot jet flames respectively, and the scalar gradient statistics have been found to be qualitatively consistent with previous findings in canonical configurations [4-8]. It is worth noting that all the aforementioned analyses have been conducted for atmospheric pressures but in many engineering applications (e.g. automotive engines and gas turbines) combustion takes place at elevated pressures. Thus, it is essential to assess if the statistical behaviours of strain rates and their influences on the SDF in turbulent premixed flames at elevated pressure remain qualitatively similar to the corresponding statistics for atmospheric flames. This motivated the current analysis which focuses on the analysis of the SDF transport statistics in turbulent premixed flames for a Bunsen-burner configuration at different pressure values. For hydrocarbon-air flames both laminar burning velocity and flame thickness decrease with increasing pressure and thus the flame resolution for a fixed geometry becomes increasingly demanding. Further, the turbulent Reynolds number increases with increasing pressure. Focusing on the fluid-dynamical aspects and following earlier work [3-7] the chemical process is described by a single-step irreversible reaction in this work.

The focus of this paper is (i) to analyse and explain the statistics of the SDF transport and (ii) to discuss implications for modelling turbulent premixed combustion at elevated pressures.

The same DNS database that was used in Ref. [20] has been used for this analysis. Although detailed discussion on this database and numerical implementation was provided in [20], some of that information is repeated here for ensuring the self-contained nature of this paper.

The database considered in this work consists of 5 Bunsen flames with identical geometry. As a consequence, in contrast to generic planar flame studies of turbulent premixed combustion reported in the literature, the scale separation between turbulent scales and flame thickness increases with increasing pressure. Hence, the turbulent Reynolds number for cases A, B, C which have been simulated at three increasing pressure levels, increases from case A to case C. It is important to note that the velocity fluctuation normalised by laminar burning velocity has been kept constant for cases A-C. In order to isolate the effects of turbulent Reynolds number from the effects of pressure variation two additional cases are considered: Bunsen Flames D and E have the same pressure as that of case A but the same turbulent Reynolds number as the highest pressure flame, case C. This is achieved by increasing the velocity fluctuation (the turbulent length scale) for case D (case E). Instantaneous views of $\tilde{c}$ iso-surface for cases A-E are shown in Fig. 1.

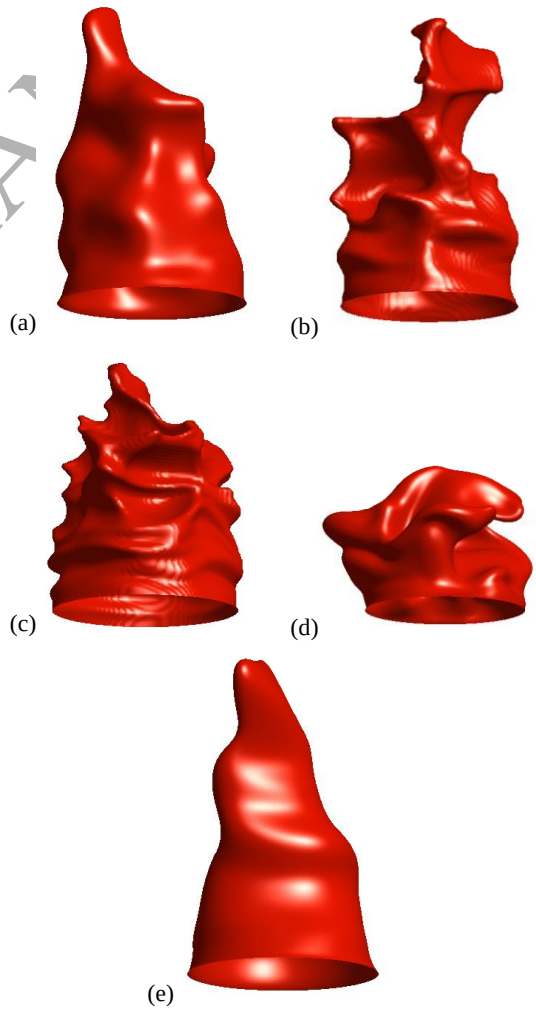

Figure 1: Instantaneous view of $\tilde{c}$ isosurface for cases (a-e) A-E.

2. MATHEMATICAL BACKGROUND

Increasing the pressure for a fixed Bunsen burner geometry is computationally expensive as the flame resolution becomes increasingly demanding and a parametric study using detailed chemistry DNS becomes prohibitively expensive [21]. Hence, a generic single-step Arrhenius type irreversible chemical mechanism is used for the current analysis. For methane-air combustion, the variation of the unstrained laminar burning velocity S_L with pressure p can be expressed as: $S_L \propto p^{-0.5}$ [22], whereas dynamic viscosity μ does not change with pressure but gas density ρ increases with pressure. This implies that the thermal flame thickness $\delta_{th} = (T_{ad} - T_0)/\max|\nabla \hat{T}|_L$ (where $\hat{T}$, T_0 and T_{ad} are the instantaneous dimensional, unburned gas and adiabatic flame temperatures respectively) scales as: $\delta_{th} \propto \mu/\rho S_L \propto p^{-0.5}$. In this analysis, the pre-exponential factor and kinematic viscosity have been modified to analyse the fluid-dynamical aspects of the pressure dependence in accordance with the aforementioned scalings.

The SDF $|\nabla c|$ and the flame surface area $\delta A = |\nabla c|\delta V$ are related quantities and there transport equations are given as [13-17]:

$$\frac{1}{|\nabla c|}\frac{\tilde{D}|\nabla c|}{\tilde{D}t} = -a_N^{eff} = -\left(a_N + N_i \frac{\partial S_d}{\partial x_i}\right) \quad (1)$$

$$\frac{1}{\delta A}\frac{\tilde{D}\delta A}{\tilde{D}t} = a_T^{eff} = a_T + 2S_d\kappa_m \quad (2)$$

where the derivative $\tilde{D}/\tilde{D}t$ has been defined as

$$\tilde{D}(\ )/\tilde{D}t = \partial(\ )/\partial t + V_j\,\partial(\ )/\partial x_j \quad (3)$$

with u_j and $V_j = u_j + S_d N_j$ being the j[th] component of the fluid velocity and flame propagation velocity respectively. In eqs. (1) and (2), S_d denotes the displacement speed defined in eq. (5). Using the flame normal vector whose j[th] component is given by $N_j = -(\partial c/\partial x_j)/|\nabla c|$ fluid-dynamic strain rate can be decomposed into flame normal a_N and tangential a_T components, given by

$$a_N = N_i N_j\,\partial u_i/\partial x_j \quad ; \quad a_T = (\delta_{ij} - N_i N_j)\,\partial u_i/\partial x_j \quad (4)$$

Finally $\kappa_m = 0.5\,\partial N_i/\partial x_i$ is the arithmetic mean of two principal curvatures. According to the current convention, the flame normal vector points towards the reactants and the flame surface convex to the reactants has a positive curvature. The flame displacement speed S_d and its components are defined as [23,24]:

$$S_d = \frac{\dot{w} + \nabla\cdot(\rho D \nabla c)}{\rho|\nabla c|} = S_r + S_n + S_t \quad (5)$$

$$S_r = \frac{\dot{w}}{\rho|\nabla c|}; \quad S_n = \frac{\vec{N}\cdot\nabla(\rho D \vec{N}\cdot\nabla c)}{\rho|\nabla c|}; \quad S_t = -2D\kappa_m \quad (6)$$

Here $\dot{w}$ is the reaction rate of reaction progress variable, and S_r, S_n and S_t are the reaction, normal diffusion and tangential diffusion components of displacement speed, respectively [23,24].

Dopazo and co-workers [13-17] referred a_N^{eff} and a_T^{eff} to as the effective normal strain rate and effective tangential strain rate respectively, whereas $N_i\,\partial S_d/\partial x_i$ and $2S_d\kappa_m$ are termed as the additional normal and tangential strain rates respectively. It is also worth noting that a_T^{eff} is alternatively known as the flame stretch rate [25,26]. The statistics of fluid-dynamic and effective strain rates in the Bunsen burner configuration at different pressures will be discussed in detail in Section 4 of this paper.

3. NUMERICAL IMPLEMENTATION

The simulations have been carried out in this analysis using the well-known compressible DNS code SENGA [27] and the numerical implementation pertinent to this analysis has been discussed elsewhere in detail [20] and thus will not be repeated here. Five different turbulent Bunsen burner flame cases (i.e. cases A-E) have been considered for this analysis. The turbulent Reynolds Re_t, integral length scale to thermal flame thickness ratio l_{11}/δ_{th}, Damköhler number Da and Karlovitz number Ka are listed in Table 1 for cases A-E. The length scale l_{11} refers to the longitudinal integral length scale of inflow turbulence prescribed at the nozzle. All the non-dimensional parameters are defined as

$$Re_t = \frac{\rho_0 u' l_{11}}{\mu_0}, \quad Da = \frac{l_{11} S_L}{u' \delta_{th}}, \quad Ka = \left(\frac{u'}{S_L}\right)^{3/2}\left(\frac{l_{11}}{\delta_{th}}\right)^{-1/2} \quad (7)$$

with ν_0 being the kinematic viscosity in the unburned gas. The bulk inflow velocity is given by $\bar{U}/S_L = 6$ in all cases. The inlet value of u'_{inlet}/S_L has been set to 1.0, except for case D where it is set to 3.1. The integral length of the inflow turbulence has been chosen according to $l_{11}/D = 1/5$ for cases A-D and $l_{11}/D = 3/5$ for case E. The heat release parameter $\tau = (T_{ad} - T_0)/T_0$, the Zel'dovich number $\beta = T_{ac}(T_{ad} - T_0)/T_{ad}^2$, where T_{ac} is the activation temperature, Prandtl number Pr and ratio of specific heats γ_g are also provided in Table 1. The reference pressure p_0 is taken to be the atmospheric pressure. All the non-dimensional numbers mentioned before have to be understood as inlet values here and in the remainder of the text. Table 1 shows that cases A-C have different values of Re_t, Da and Ka and thus they belong to the different locations on the combustion regime diagram.

Case	p/p_0	Re_t	l_{11}/δ_{th}	Da	Ka
A	1.0	13.30	5.20	0.45	5.00
B	5.0	29.26	11.40	0.30	11.40
C	10.0	41.22	16.13	0.25	16.13
D	1.0	41.22	5.20	2.40	1.670
E	1.0	41.22	16.13	0.25	16.13
$\tau = 4.5$ $\beta = 6.0$ $Pr = 0.7$ $\gamma_g = 1.4$					

Table 1: Attributes of inlet turbulence and thermochemistry for the cases considered here

It is worth noting that cases A-C and E fall on the boundary of the wrinkled and the corrugated flamelets regimes according to the regime diagram by Peters [28]. Table 1 shows that cases C, D and E have same values of Re_t but cases D and E have one tenth of the pressure of that of case C. The value of u'/S_L is higher in case D than in case C and E, whereas u'/S_L and l_{11}/δ_{th} values are exactly the same for cases C and E, and thus they fall on the same point on the regime diagram. The reader is also referred to Fig.1 in [20]. The simulation domain is taken to be $2D \times 2D \times 2D$ which corresponds to a cube of $50\delta_{th} \times 50\delta_{th} \times 50\delta_{th}$ [$112\delta_{th} \times 112\delta_{th} \times$

ρρς for cases A, D and E [case B] (case C) which is discretised using a uniform Cartesian grid of 250×250×250 [560×560×560] (795×795×795) points, ensuring the resolution of both the Kolmogorov length scale and the flame thickness. The statistics have been extracted after 2 through pass times (i.e. where is the length of the simulation domain) and at least 10 different realisations have been utilised to extract the statistics reported in the next section of this paper.

4. RESULTS & DISCUSSION

4.1 Flame-turbulence interaction

The instantaneous views of iso-surface for cases A-E are shown in Fig. 1 and this isosurface can be considered as the flame surface because the maximum reaction rate occurs close to for the present thermo-chemistry. The nature of flame wrinkling for cases A-C is different from each other. It has been discussed elsewhere [20] that the normalised flame surface area assumes similar values in cases A-C but it can be seen from Fig. 1 that the probability of obtaining sharply negative cusps between positively curved bulges increases from case A to case C. It has been discussed elsewhere [20,29] that case C exhibits Darrieus-Landau (DL) instability, whereas this effect is either absent or weak in cases A and B. This gives rise to the aforementioned differences in flame wrinkling. Figure 1 further shows that flame morphologies for cases C-E are different in spite of the inlet flow having the same turbulent Reynolds number for these cases. For example, the flame in case E is less wrinkled in comparison to case C, although both cases share the same position on the regime diagram. The flame in case D also shows greater extent of flame wrinkling than case E because of higher value in case D. The greater extent of flame wrinkling in cases C and D than in case E is reflected in the higher value of which can be substantiated from Table 2 of Ref. [20].

It can be seen from Fig. 1 that the flame wrinkling changes with axial distance and thus the SDF transport statistics in this paper have been analysed for different axial locations. The cuts of flame heights considered in this analysis are 0.2, 0.4 and 0.6 of nozzle diameter and these axial height locations are referred to as H1, H2 and H3 respectively.

4.2. Statistical behaviour of and

The profiles of the mean variation of normalised SDF conditional upon for cases A-E is exemplarily shown in Fig. 2 for H2 and the same trend was observed for all axial locations and also for the corresponding variation using the samples from the whole domain.

The peak value of the conditional mean value of the SDF provides a measure of the flamelet thickness (i.e. , where is the flamelet thickness) in turbulent combustion [8]. For a low Mach number globally adiabatic combustion with unity Lewis number, the reaction progress variable can be equated to the non-dimensional temperature . Hence, the thermal flame thickness can alternatively be defined as:. Therefore, the maximum value provides a measure of the ratio of laminar flame thickness to turbulent flamelet thickness. A peak conditional mean value of with a value greater (smaller) than unity indicates an instance of flame thinning (thickening) under turbulent conditions. It can be seen from Fig. 2 that the peak value of the conditional mean of assumes a value which is marginally greater than 1.0, which suggests a small amount of flame thinning under turbulence for these flames. Flame thinning under turbulence is consistent with previous findings by Soika *et al.* [30] and Hawkes *et al.* [31] but other analyses [8,32-34] in the thin reaction zones regime reported flame thickening under turbulent conditions. It is worth mentioning (but not shown for the sake of brevity) that the mean behaviour of SDF conditional upon does not significantly change with the flame height.

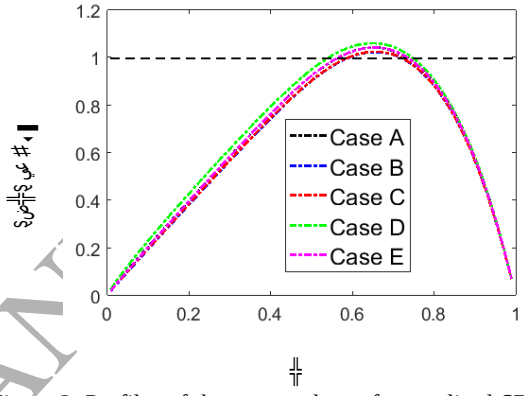

Figure 2: Profiles of the mean values of normalised SDF conditional upon for cases A to E (shown by -.- here and in the rest of the paper).

It is important to analyse the statistical behaviours of and its components in order to understand the SDF statistics further. The mean behaviours of and have been discussed elsewhere [20] and thus will not be repeated here. Previous analysis indicated that mean behaviours of conditional and and its components for cases A-E are qualitatively and quantitatively similar to each other, and these variations also do not change significantly with the axial distance. The mean behaviours of conditional on are both qualitatively and quantitatively similar for cases A-C and E [20]. However, the extent of alignment of with the most extensive principal strain rate in case D is smaller than the other cases and thus the mean value of conditional on in case D assumes smaller value than the corresponding value in the other cases [20]. The DL instability has been shown to affect the mean behaviour of due to the correlation between dilatation rate and curvature. The mean value of is the smallest in case C amongst the cases considered here because of the defocussing of heat at the positively curved bulges arising from the DL instability [20]. The mean behaviours of and have also been found to remain unchanged with axial distance. Interested readers are referred to Ref. [20] for further explanations of these behaviours. The mean behaviour of tangential strain rate is determined by the relative magnitudes of the mean values of both dilatation rate and normal strain rate. The mean value of remains positive throughout the flame front and

the highest (lowest) magnitude of the mean value of $\tilde{\omega}_1$ is obtained for case D (case C). Further discussion on the mean normalised tangential strain rate $\tilde{\omega}_1$ can be found as well in Ref. [20]. This paper will henceforth concentrate on the statistical behaviours of $\tilde{\kappa}_c$ and $\zeta_{\parallel c}$, which are the normal strain rate induced by the flame propagation, and curvature stretch (which alternatively can be seen as the tangential strain rate induced by flame propagation [13-17]), respectively.

4.3 Statistical behaviour of additional strain rates due to flame propagation

The mean values of $\tilde{\kappa}_c \tilde{N}_c \tilde{\omega}_c$, $\tilde{\kappa}_c \tilde{N}_h \tilde{\omega}_c$, $\tilde{\kappa}_c \tilde{N}_t \tilde{\omega}_c$ and $\tilde{\kappa}_c \tilde{N}_n \tilde{\omega}_c$ conditional on $\tilde{\omega}$ are shown in Fig. 3 exemplarily for case C and other cases are not shown for the sake of brevity because they exhibit similar behaviour. The normalised reaction component of displacement speed $\tilde{N}_h$ assumes positive values throughout the flame and its magnitude increases from the unburned to the burned gas side of the flame (i.e. in the direction opposite to the flame normal) and thus the contribution of $\tilde{\kappa}_c \tilde{N}_h \tilde{\omega}_c$ assumes a negative value throughout the flame. The mean contribution of $\tilde{\kappa}_c \tilde{N}_h \tilde{\omega}_c$ assumes small (large) negative (positive) values on the unburned (burned) gas side of the flame front due to predominantly positive (negative) values of $\tilde{N}_h$ [20]. The magnitude of the mean contribution of $\tilde{\kappa}_c \tilde{N}_t \tilde{\omega}_c$ remains negligible in comparison to that of $\tilde{\kappa}_c \tilde{N}_h \tilde{\omega}_c$ and $\tilde{\kappa}_c \tilde{N}_h \tilde{\omega}_c$ and the relative magnitudes of the mean contributions of $\tilde{\kappa}_c \tilde{N}_h \tilde{\omega}_c$ and $\tilde{\kappa}_c \tilde{N}_h \tilde{\omega}_c$ determine the mean value of $\tilde{\kappa}_c \tilde{N}_n \tilde{\omega}_c$, which remains negative throughout the flame for all cases considered here. Moreover, there is little difference in the mean values of $\tilde{\kappa}_c \tilde{N}_b \tilde{\omega}_c$ (i.e. $\langle \cdot \rangle_{sl}$) for cases A-E. Thus, both pressure and turbulent Reynolds number variations for this parameter range do not significantly affect the mean behaviour of additional normal strain rate $\tilde{\kappa}_c \tilde{N}_n \tilde{\omega}_c$ arising from flame propagation. Although not shown in Fig. 3, it is mentioned, that the mean values of $\tilde{\kappa}_c \tilde{N}_b \tilde{\omega}_c$ (i.e. $\langle \cdot \rangle_{sl}$) are not affected by the axial distance from the burner exit and in fact the profiles for axial locations H1, H2 and H3 cannot be distinguished from each other.

Case C

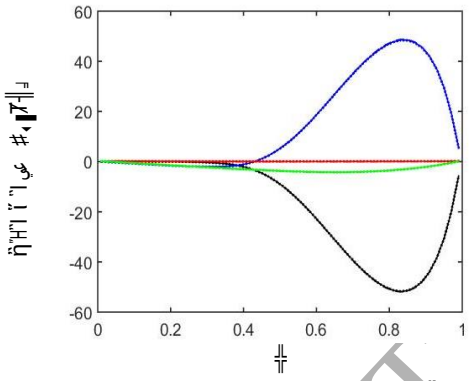

Figure 3: Profiles of the mean values of $\tilde{\kappa}_c \tilde{N}_c \tilde{\omega}_c$ (black), $\tilde{\kappa}_c \tilde{N}_h \tilde{\omega}_c$ (blue), $\tilde{\kappa}_c \tilde{N}_t \tilde{\omega}_c$ (red) and $\tilde{\kappa}_c \tilde{N}_n \tilde{\omega}_c$ (green) conditional upon $\tilde{\omega}$ for case C at axial locations H1 (- - -), H2(-.-) and H3 (…..).

The mean values of $\zeta \tilde{N}_c \tilde{N}_h \| \tilde{\omega}$, $\zeta \tilde{N}_t \| \tilde{\omega}$ and $\zeta \tilde{N}_n \| \tilde{\omega}$ conditional on $\tilde{\omega}$ are shown in Fig. 4. It can be seen from Fig. 4 that the mean contribution of $\zeta \tilde{N}_t \| \tilde{\omega}$ remains small in comparison to $\zeta \tilde{N}_c \tilde{N}_h \| \tilde{\omega}$ in cases A-C and E, and the mean behaviour of $\zeta \tilde{N}_n \| \tilde{\omega}$ in these cases is governed by $\zeta \tilde{N}_c \tilde{N}_h \| \tilde{\omega}$. However, in case D the mean contribution of $\zeta \tilde{N}_t \| \tilde{\omega}$ is comparable to that of $\zeta \tilde{N}_c \tilde{N}_h \| \tilde{\omega}$ and thus both $\zeta \tilde{N}_t \| \tilde{\omega}$ and $\zeta \tilde{N}_c \tilde{N}_h \| \tilde{\omega}$ remain significant contributors to $\zeta \tilde{N}_n \| \tilde{\omega}$.

The flames considered here have negative mean curvatures [20,29], whereas the mean $\tilde{N}_c \tilde{N}_h$ remains positive throughout the flame front for all cases considered here [20]. Furthermore, the correlation between $\tilde{N}_c \tilde{N}_h$ and $\|_c$ remains weakly negative throughout the flame, which can be seen from the correlation coefficients between $\tilde{N}_c \tilde{N}_h$ and $\|_c$ listed in Table 2 based on the samples over the whole flame. It is worth noting that the qualitative nature of the correlation between $\tilde{N}_c \tilde{N}_h$ and $\|_c$ remains unchanged throughout the length of the flame (not shown here). The weak negative correlation between $\tilde{N}_c \tilde{N}_h$ and $\|_c$ is consistent with several previous analyses [6-9,35-38] where physical explanations for this behaviour were provided and thus are not repeated here. This weak negative correlation between $\tilde{N}_c \tilde{N}_h$ and $\|_c$ along with predominantly positive and negative values of $\tilde{N}_c \tilde{N}_h$ and $\|_c$ respectively leads to a negative mean value of $\zeta \tilde{N}_c \tilde{N}_h \| \tilde{\omega}$. As the flame curvature $\|_c$ and the correlation between $\tilde{N}_c \tilde{N}_h$ and $\|_c$ change with the flame height, the mean behaviour of $\zeta \tilde{N}_c \tilde{N}_h \| \tilde{\omega}$ also exhibits an axial distance dependence but the qualitative behaviour remains unchanged.

Case A **Case B**

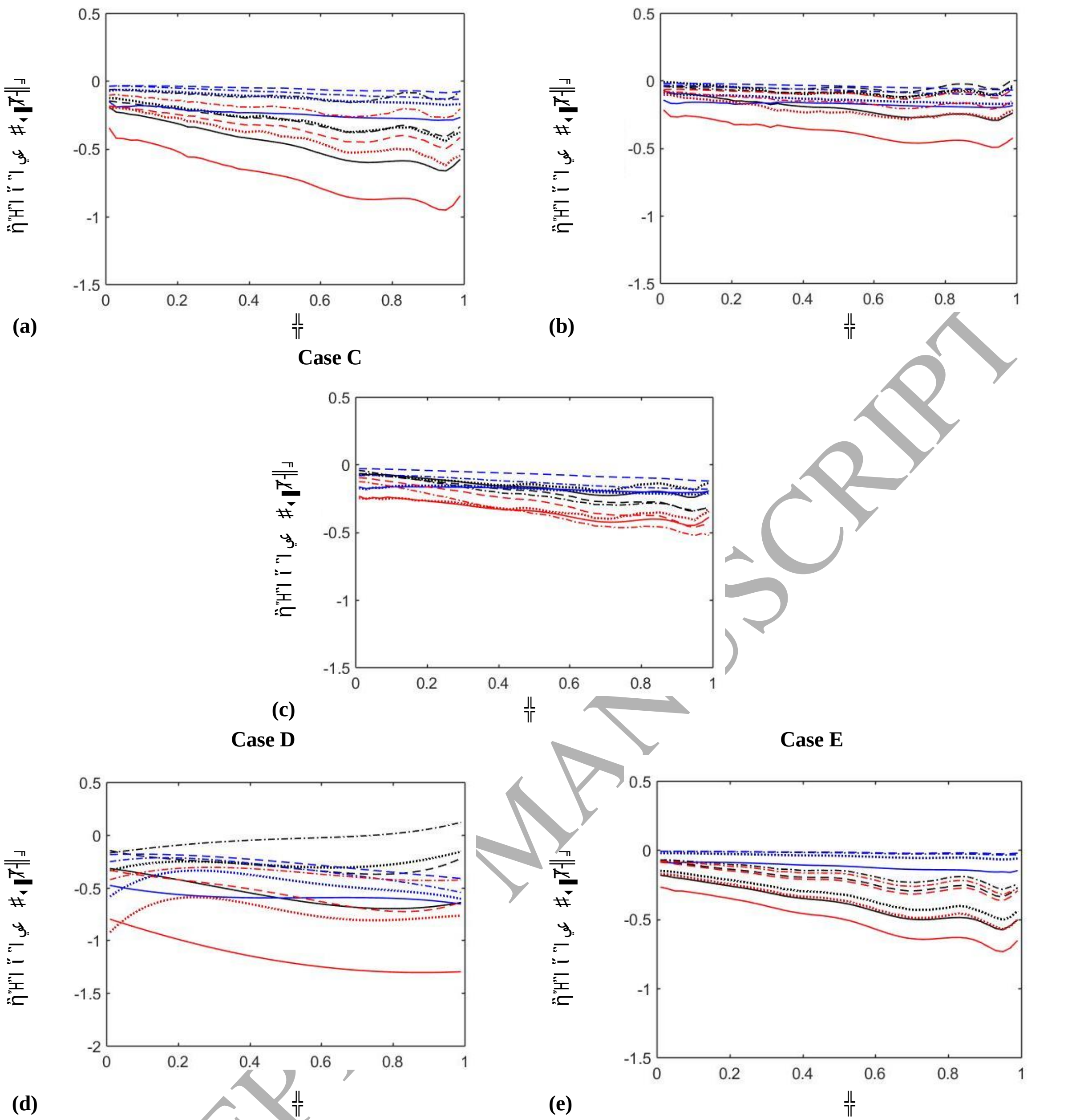

Figure 4: Profiles of the mean values of [illegible] (black), [illegible] (blue) and [illegible] (red) conditional upon [illegible] for cases (a-e) A-E at different axial locations.

Case	[illegible]	[illegible]	[illegible]	[illegible]	[illegible]
A	-0.55	-0.45	-0.31	-0.20	0.05
B	-0.60	-0.51	-0.36	-0.23	-0.03
C	-0.59	-0.53	-0.43	-0.32	-0.14
D	-0.30	-0.26	-0.19	-0.09	0.03
E	-0.59	-0.48	-0.30	-0.21	0.09

Table 2: Correlation coefficients between [illegible] and [illegible] for [illegible] isosurface for all cases considered here. Here the mean correlation coefficient based on all the different realisations is shown.

The term [illegible] is deterministically negative. According to Peters [28] the influences of tangential diffusion component of displacement speed [illegible] are expected to be weak in comparison to the combined actions of reaction and normal diffusion components of displacement speed

ͮ ط ͮ for small values of Karlovitz number (i.e. ݇ܽ ح ρ) as cases A-C and E considered here. Thus, in these cases the mean value of ςͮ‖ عي ۱ ژ ڸ ͮ has been found to be smaller than the mean contribution of ς ͮ ط ͮ ‖ عي ۱ ژ ڸ ͮ , which is in contrast to dominant contribution of ςͮ‖ due to ςͮ‖ in the thin reaction zones regime flames (where ݇ܽ حي ρ) [37,39]. Case D belongs nominally to the thin reaction zones regime combustion (i.e. ݇ܽ حي ρ) where the influence of tangential diffusion component of displacement speed ͮ is expected to be strong and thus the mean value of ςͮ‖ عي ۱ ژ ڸ ͮ becomes comparable to the mean contribution of ς ͮ ط ͮ ‖ عي ۱ ژ ڸ ͮ . The contribution of ςͮ‖ عي ۱ ژ ڸ ͮ is expected to strengthen with increasing values of ݇ܽ and to become the major contributor to ςͮ‖ عي ۱ ژ ڸ ͮ for large values of ݇ܽ as demonstrated in previous analyses [37,39]. As the curvature distribution changes with axial distance, the mean behaviour of ςͮ‖ عي ۱ ژ ڸ ͮ طي سي τΌ‖ عي ۱ ژ ڸ ͮ also exhibits quantitative variation with the flame height.

Figure 4 shows that the magnitudes of the mean values of ς ͮ ط ͮ ‖ عي ۱ ژ ڸ ͮ and ςͮ‖ عي ۱ ژ ڸ ͮ are greater in case A (case B) than in case B (case C). The probability of finding positive values of ‖ increases from case A to C, which acts to reduce the magnitude of the negative mean value of ς ͮ ط ͮ ‖ عي ۱ ژ ڸ ͮ , which also leads to a reduction in the magnitude of the mean value of ςͮ‖ عي ۱ ژ ڸ ͮ from case A to C. It is worth noting that the differences in curvature distributions arise primarily due to the influences of the DL instability for high pressure flames, and the DL instability is principally responsible for the observed change in the mean behaviour of the curvature stretch rate ςͮ‖ [25,26] (or additional tangential strain rate [13-17]) from one case to another. The mean contribution of ςͮ‖ عي ۱ ژ ڸ ͮ becomes comparable to that of ς ͮ ط ͮ ‖ عي ۱ ژ ڸ ͮ in case D (see Fig. 4), and thus the negative mean value of ςͮ‖ عي ۱ ژ ڸ ͮ shows the highest magnitude in this case among the flames considered here. A change in combustion regime is principally responsible for the difference in behaviour of ςͮ‖ عي ۱ ژ ڸ ͮ in case D in comparison to the other cases.

4.4 Statistical behaviour of effective strain rates

The mean values of ܽ عي ۱ ژ ڸ ͮ , ܷ ͮ ܽ عي ۱ ژ ڸ ͮ , and ܽ عي ۱ ژ ڸ ͮ سي ܽ ط ܷ ͮ ܽ عي ۱ ژ ڸ ͮ conditional on ܽ are shown in Fig. 5. Case B behaves very similar to case C and is not shown for the sake of brevity. It can be seen that the positive mean values of ܽ عي ۱ ژ ڸ ͮ almost nullify the negative mean values of ܷ ͮ ܽ عي ۱ ژ ڸ ͮ to yield negligible mean values of ܽ for all cases considered here. The differences in mean values of ܽ between all cases is much smaller than the standard deviation of ܽ (not shown here), and thus this difference cannot be attributed to any physical effects. It has been demonstrated earlier that pressure and turbulent Reynolds number variations do not significantly affect the mean behaviours of ܽ عي ۱ ژ ڸ ͮ (see Fig. 5) within the parameter range considered here, and thus the effective normal strain rate ܽ عي ۱ ژ ڸ ͮ also does not exhibit any significant ܲ and ͮΩ dependence.

Moreover, the mean values of ܽ عي ۱ ژ ڸ ͮ , and ܷ ͮ ܽ عي ۱ ژ ڸ ͮ , are not affected by the axial distance from the burner exit (see Fig. 5) and thus ܽ عي ۱ ژ ڸ ͮ also does not exhibit any significant dependence on the flame height. The negligible mean value of ܽ suggests that the mean value of ȘܽȘ Ω ȘܽȘΩ remains negligible in these flames according to eqs. 1 and 2, and thus the mean ȘܽȘ profile remains almost similar to that of a planar laminar flame for all cases considered here. This can be confirmed from Fig. 6 where ȘܽȘ ȘܽȘ conditional on ܽ for both laminar and turbulent flames is shown with ȘܽȘ being the peak mean value of ȘܽȘ conditional upon ܽ. In Fig. 6, only case C is exemplarily shown for the sake of brevity because other cases behave in a similar manner. The similarity of ȘܽȘ profiles between laminar and turbulent flames is consistent with the fact that the flamelet thickness in these turbulent flames remains almost the same as the laminar flame thickness.

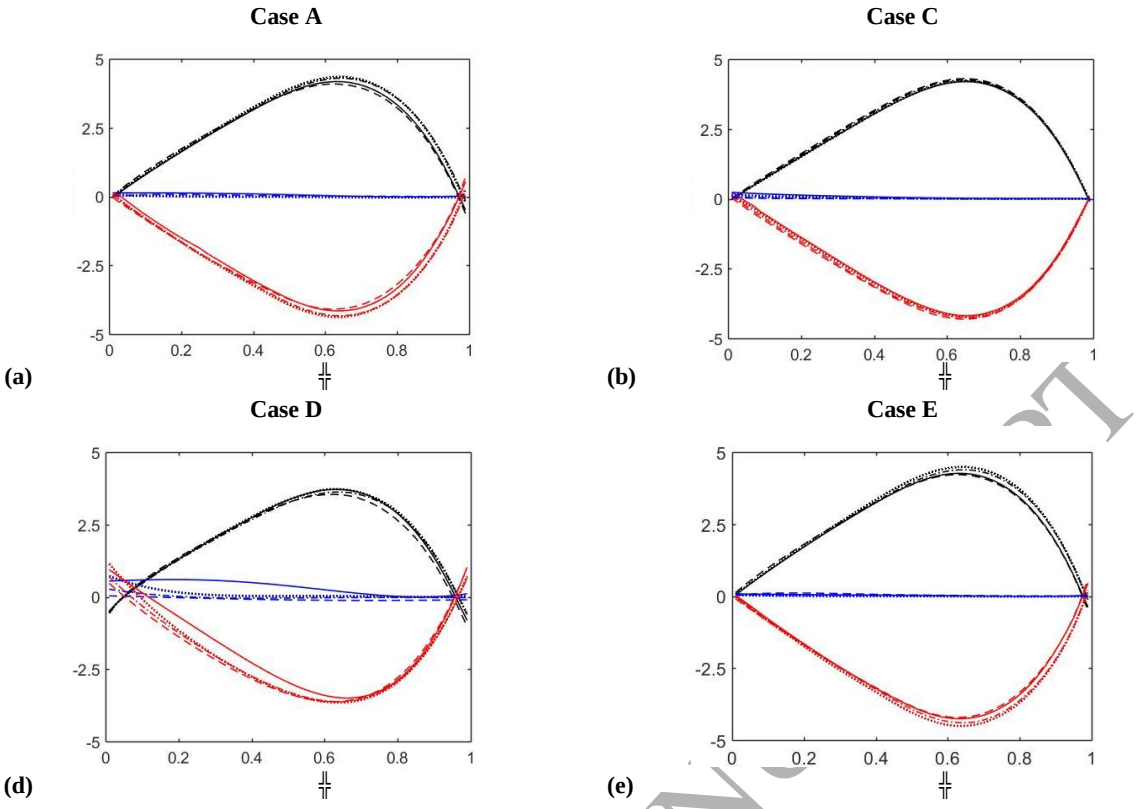

Figure 5: Profiles of the mean values of $\tilde{\omega}_1$ (in black), $\tilde{\omega}_2$ (in red) and $\tilde{\omega}_1^{sdr}$ (in blue) conditional upon $\tilde{\omega}$ for cases (a-d) A,C,D,E at different axial locations (same legend as in Fig. 4).

The mean values of $\tilde{\omega}_1$, ζ_2, and $\tilde{\omega}_1^{sdr}$ conditional on $\tilde{\omega}$ are shown in Fig. 7, which suggests that $\tilde{\omega}_1$ and ζ_2 almost cancel each other so that the mean flame stretch (or effective tangential strain rate) $\tilde{\omega}_1^{sdr}$, based on the samples obtained from the whole flame remains small for all cases considered here. However, there is a large amount of scatter around these mean values for all cases (not shown here) and thus the small difference in the mean values of $\tilde{\omega}_1^{sdr}$ based on the samples from the whole flame should not be attributed to the pressure variation.

The mean behaviour of $\tilde{\omega}_1^{sdr}$ does not show significant dependence on the flame height for cases A-C and E but in case D non-negligible positive mean value of $\tilde{\omega}_1^{sdr}$ at locations H1, H2 and H3 can be observed where high values of $\tilde{\omega}_1$ dominate over ζ_2. It has been discussed earlier and also in Ref. [27] that the differences in behaviours of ζ_2 and $\tilde{\omega}_1$ between case D and the other cases originate due to the fact that case D belongs to a different regime of combustion and not because of pressure variation.

The similarity in the conditional mean values of $\tilde{\omega}_1^{sdr}$ based on the whole domain also contributes to the similar values of $\langle \Sigma \rangle$ (see Table 2 of Ref. [20]) because (i) the initial normalised laminar flame surface areas $\langle \Sigma_0 \rangle$ remains the same for all cases as $\tilde{c}$ and $\langle \dot{\omega}_c \rangle$ are kept unaltered for all the cases considered here, (ii) both $\langle \dot{\omega}_c \rangle$ and l_F scale with $\tilde{u}'^{3}$ so $\langle \dot{\omega}_c \rangle l_F$ (i.e. the normalisation used) remains independent of $\tilde{u}'$. Thus the fractional change in area according to eq. 2 remains similar for all cases considered here.

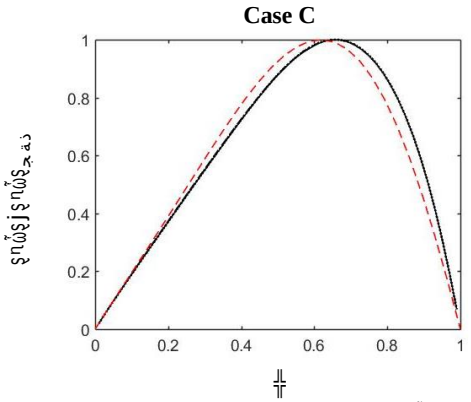

Figure 6: Profiles of the mean values of $\tilde{n}_3 | \tilde{n}_3 \tilde{n}_3$ conditional upon $\tilde{\omega}$ for case C at different axial locations. The red broken line shows the laminar flame solution. The turbulent flame results are shown in black (same colour key as in Fig. 4, note that several lines hide each other).

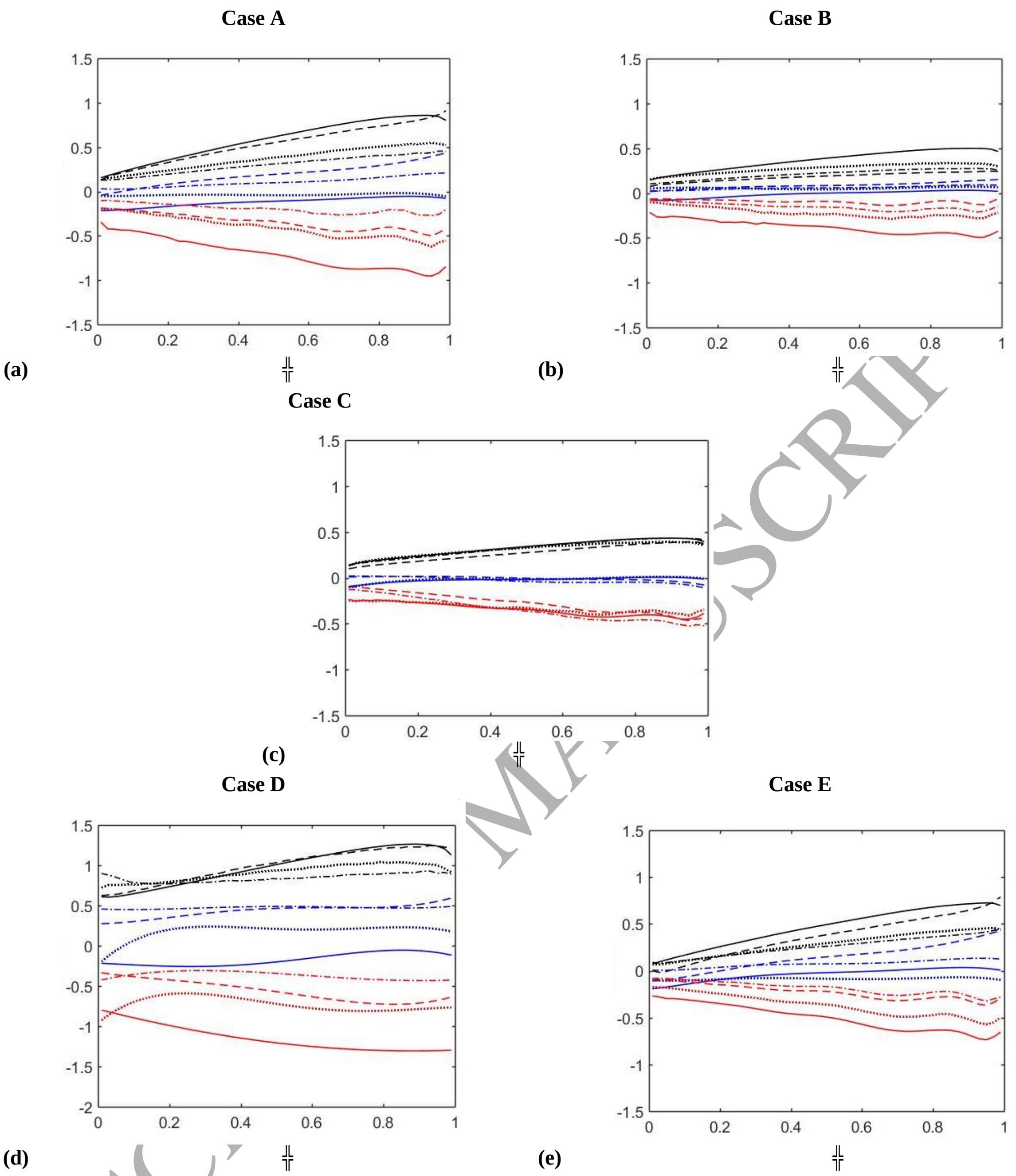

Figure 7: Profiles of the mean values of [illegible] (black), [illegible] (red) and [illegible] (blue) conditional upon [illegible] for cases (a-e) A-E at different axial locations.

Case	p/p_0	$\mu(\Omega)$	$\sigma(\Omega)$
A	1.0	4.49	0.39
B	5.0	4.60	0.42
C	10.0	4.56	0.15
D	1.0	4.53	0.46
E	1.0	4.10	0.21

Table 3: Normalised burning rate $\Omega = \int_V \dot{\omega}\, dV / (\rho_0 S_L A_L)$ for the cases considered here. Here $\mu(Q)$ and $\sigma(Q)$ are the mean and standard deviation of a quantity Q based on different realisations.

Although both a_T and $2S_d\kappa_m$ are affected by the DL instability for the high pressure flame (i.e. case C), the reduced probability of having large positive values of a_T is partially nullified by the predominance of small negative values of $2S_d\kappa_m$. However, greater extent of flame wrinkling in case C due to the DL instability yields higher flame surface area than in case E. Moreover, high mean positive $a_T \times \delta_{th}/S_L$, in case D is partially nullified by the high negative mean values of $2S_d\kappa_m \times \delta_{th}/S_L$, and this brings the mean value of $a_T^{eff} \times \delta_{th}/S_L$, to a level which is comparable to the corresponding values in the other cases. This closeness in flame surface area values in between the cases considered here is expected to give rise to the similarity in the normalized burning rate $\Omega = \int_V \dot{\omega}\, dV/(\rho_0 S_L A_L)$ as all the flames considered here exhibit flamelet combustion and thus the consumption rate per unit flame area can be scaled with $\rho_0 S_L$. This can be substantiated from Table 3 where the values of mean and standard deviation of normalised burning rate Ω based on different realisations of cases A-E are listed. However, case C shows higher value of Ω than in case E due to greater flame surface area in case C (see Table 2 of Ref. [20]). This indicates that the pressure variation does not have any major influence on normalised flame surface area and burning rate values but the DL instability is likely to occur at high pressure flames (e.g. case C) which are expected to show higher values of burning rate and flame surface area than the corresponding low pressure flames where the DL instability is absent (e.g. case E).

4.5 Local behaviour and modelling implications

The mean behaviours of $N_j \partial S_d/\partial x_j$, $2S_d\kappa_m$, a_N^{eff} and a_T^{eff} have been discussed in the previous sub-sections but also the local curvature and strain rate dependences of these quantities remain qualitatively similar for all cases considered here. This can be substantiated from the correlation coefficients listed in Table 4. The joint pdfs corresponding to the correlation coefficients are not shown here for the sake of conciseness. Table 4 indicates that the variations of pressure and turbulent Reynolds number do also not affect the qualitative nature of local behaviours of $N_j \partial S_d/\partial x_j$, $2S_d\kappa_m$, a_N^{eff} and a_T^{eff}. The present analysis suggests that the variation of pressure does not have significant influences on the statistical behaviours of a_T [20], $N_j \partial S_d/\partial x_j$, and a_T^{eff}. It has been demonstrated elsewhere [20] that the DL instability affects the mean behaviours of a_T and the present analysis shows that the DL instability also affects the mean behaviour of $2S_d\kappa_m$. However, these effects counter each other to some extent and consequently $a_T^{eff} \times \delta_{th}/S_L (= a_T + 2S_d\kappa_m \times \delta_{th}/S_L)$ does not exhibit any significant pressure dependence.

The transport equation of $|\nabla c|$ can be written by expanding eq. 1:

$$\frac{\partial|\nabla c|}{\partial t} + u_j \frac{\partial|\nabla c|}{\partial x_j} = -a_N^{eff}|\nabla c| - S_d N_j \frac{\partial|\nabla c|}{\partial x_j} \quad (8i)$$

which can alternatively be written as:

$$\frac{\partial|\nabla c|}{\partial t} + \frac{\partial (u_j|\nabla c|)}{\partial x_j} = a_T^{eff}|\nabla c| + 2S_d\kappa_m|\nabla c| + N_j \frac{\partial N_j}{\partial x_j}|\nabla c| S_d - N_j \frac{\partial (S_d|\nabla c|)}{\partial x_j} \quad (8ii)$$

It is possible to obtain the transport equation of the generalised FSD (i.e. $\Sigma_{gen} = \overline{|\nabla c|}$) [2] on Reynolds averaging/LES filtering eqs. 8i and 8ii. Algebraic manipulation of eq. 8 provides the transport equation of scalar dissipation rate (SDR) $N_c = D|\nabla c|^2$ [20]:

$$\frac{\partial N_c}{\partial t} + \frac{\partial (u_j N_c)}{\partial x_j} = -2a_N^{eff} N_c + \rho S_d N_j \frac{\partial N_c}{\partial x_j} + [\text{illegible}] \quad (9)$$

It is evident from eqs. 8 and 9 that the transports of FSD and SDR are strongly dependent on $N_j \partial S_d/\partial x_j$, $2S_d\kappa_m$, a_N^{eff} and a_T^{eff}. As the present findings indicate that the pressure variation does not significantly affect the statistics of $N_j \partial S_d/\partial x_j$, $2S_d\kappa_m$, a_N^{eff} and a_T^{eff}, the models for FSD and SDR transports, which were proposed for atmospheric condition, may also work for elevated pressure conditions at least in the flamelet regime of combustion, provided the influences of the DL instability on a_T and $2S_d\kappa_m$ are appropriately accounted for.

Case	$N_j \partial S_d/\partial x_j$	$2S_d\kappa_m$	a_N^{eff}	a_T^{eff}
A	0.07	0.91	0.85	-0.07
B	0.00	0.96	0.90	-0.05
C	-0.06	0.94	0.87	-0.10
D	0.10	0.88	0.79	-0.07
E	0.17	0.95	0.88	0.00

Table 4: Correlation coefficients between curvature κ_m and different strain rate components (i.e. $N_j \partial S_d/\partial x_j$, $2S_d\kappa_m$, a_N^{eff} and a_T^{eff}). Here the mean correlation coefficient based on all the different realisations is shown.

5. CONCLUSIONS

The statistical behaviours of the SDF and its transport have been analysed based on three-dimensional compressible simple chemistry DNS simulations of turbulent Bunsen burner flames representing the flamelet regime of premixed turbulent combustion at different pressure and Reynolds number values. Both pressure and turbulent Reynolds number variations have no significant influences on the mean behaviours of the normal strain rate arising from flame propagation $\vec{N}\cdot\nabla(S_d\vec{N})$. The Darrieus-Landau (DL) instability is more likely to occur for high pressure flames and the presence of the DL instability affects the statistical behaviours of curvature stretch $S_d\nabla\cdot\vec{N}$. The influence of the DL instability on the positive mean tangential strain rate partially nullifies the effects of instability on the negative mean curvature stretch and thus the effective tangential strain rate (or net stretch rate) remains mostly unaffected by the pressure variation. The similarities in the statistical behaviours of the normalised SDF $|\nabla c|\times\delta_{th}$ and effective strain rates (i.e. $(a_N)_{eff}\times\delta_{th}/S_L$ and $(a_T)_{eff}\times\delta_{th}/S_L$), imply that existing models in the context of FSD and SDR closures, which have been validated with respect to atmospheric pressure conditions, are likely to be valid even for elevated pressures in the absence of the DL instability. However, the DL instability is likely to occur at high pressure conditions, and this is expected to influence the tangential strain rate a_T and curvature stretch $S_d\nabla\cdot\vec{N}$ contributions to the FSD and SDR transports. Based on this observation it can be argued that accurate models for the tangential strain rate and curvature stretch contributions to the FSD and SDR transports need to account for the implicit effects of the DL instability potentially occurring at elevated pressures conditions.

This analysis does not address the influences of thermo-diffusive effects associated with the non-unity Lewis number. Moreover, the current analysis focuses only on fluid-dynamical aspects of the influences of pressure on the SDF transport statistics. Earlier work reported qualitative similarities between the SDF transport [4-8, 40] statistics between simple and detailed chemistry DNS results. Nevertheless, it will be necessary to validate the current findings with detailed chemistry and transport simulations in future.

ACKNOWLEDGEMENTS

The authors are grateful to Gauss Centre for Supercomputing / Leibniz Supercomputing Centre (grant: pr74ra) and ARCHER (EP/K025163/1) for computing support.

REFERENCES

[1] W. Kollmann, J.H. Chen, Pocket formation and the flame surface density equation, Proc. Combust. Inst., 27 (1998) 927-934.

[2] M. Boger, D. Veynante, H. Boughanem, A. Trouvé, Direct Numerical Simulation analysis of flame surface density concept for Large Eddy Simulation of turbulent premixed combustion, Proc. Combust. Inst., 27 (1998) 917-925.

[3] N. Chakraborty, M. Champion, A. Mura and N. Swaminathan, Scalar dissipation rate approach to reaction rate closure. In: Turbulent premixed flame, Swaminathan, N. and Bray, K.N.C. (eds.). Cambridge University Press, 1st Edition, Cambridge, UK, pp. 76-102 (2011).

[4] N. Chakraborty, R.S. Cant, Effects of strain rate and curvature on Surface Density Function transport in turbulent premixed flames in the thin reaction zones regime, Phys. Fluids, 17 (2005) 65108.

[5] N. Chakraborty, M. Klein, Influence of Lewis number on the Surface Density Function transport in the thin reaction zones regime for turbulent premixed flames, Phys. Fluids, 20 (2008) 065102.

[6] N. Chakraborty, M. Klein, Effects of global flame curvature on the Surface Density Function transport in Turbulent premixed flame kernels in the Thin Reaction Zones regime." Proc. Combust. Inst., 32 (2009) 1435-1443.

[7] N. Chakraborty, E.R. Hawkes, J.H. Chen, R.S. Cant, Effects of strain rate and curvature on Surface Density Function transport in turbulent premixed CH_4-air and H_2-air flames: A comparative study, Combust. Flame, 154 (2008) 259–280.

[8] R. Sankaran, E.R. Hawkes, J.H. Chen, T. Lu, C.K. Law, Structure of a spatially developing turbulent lean methane–air Bunsen flame, Proc. Combust. Inst., 31 (2007) 1291-1298.

[9] N. Chakraborty, N. Swaminathan, Influence of Damköhler number on turbulence-scalar interaction in premixed flames, Part I: Physical Insight, Phys. Fluids, 19 (2007) 045103.

[10] S. H. Kim, H., Pitsch, Scalar gradient and small-scale structure in turbulent premixed combustion, Phys. Fluids, 19 (2007) 115104.

[11] N. Chakraborty, M. Klein, N. Swaminathan, Effects of Lewis number on reactive scalar gradient alignment with local strain rate in turbulent premixed flames, Proc. Combust. Inst., 32 (2009) 1409–1417.

[12] G. Hartung, J. Hult, C.F. Kaminski, J.W. Rogerson, N. Swaminathan, Effect of heat release on turbulence and scalar-turbulence interaction in premixed combustion, Phys. Fluids, 20 (2008) 035110.

[13] L. Cifuentes, C. Dopazo, J. Martin, C. Jimenez, Local flow topologies and scalar structures in a turbulent premixed flame, Phys. Fluids, 26 (2014) 065108.

[14] L. Cifuentes, C. Dopazo, J. Martin, P. Domingo, L. Vervisch, Local volumetric dilatation rate and scalar geometries in a premixed methane-air turbulent jet flame, Proc. Combust. Inst., 35 (2015) 1295–1303.

[15] C. Dopazo, L. Cifuentes, J. Martin, C. Jimenez, Strain rates normal to approaching isoscalar surfaces in a turbulent premixed flame, Combust. Flame, 162 (2015) 1729- 1736.

[16] C. Dopazo, L. Cifuentes, J. Hierro, J. Martin, J., Micro-scale mixing in turbulent constant density reacting flows and premixed combustion, Flow Turb. Combust., 96 (2015) 547-571.

[17] C. Dopazo, L. Cifuentes, The physics of scalar gradients in turbulent premixed combustion and its relevance to modeling, Combust. Sci. Technol., 188(9) (2016) 1376-1397.

[18] H. Wang, E.R. Hawkes, J. H. Chen, B. Zhou, Z. Li, M. Alden, Direct numerical simulations of a high Karlovitz number laboratory premixed jet flame- an analysis of flame stretch and flame thickening, J. Fluid Mech., 815 (2017) 511-536.

[19] S. Chaudhuri, H. Kolla, H. L. Dave, E. R. Hawkes, J. H. Chen, C. K. Law, Flame thickness and conditional scalar dissipation rate in a premixed turbulent reacting jet, Combust. Flame, 184 (2017) 273-285.

[20] M. Klein, D. Alwazzan, N. Chakraborty, A Direct Numerical Simulation analysis of pressure variation in turbulent premixed Bunsen burner flames-Part 1: Scalar gradient and strain rate statistics Comput. Fluids (under review).
[21] J.H. Chen, A. Choudhary, M. de Supinski, B. de Vries, E.R. Hawkes, S. Klasky, W.K. Liao, K.L. Ma, J. Mellor-Crummey, N. Podhorski, R. Sankaran, S. Shende and C. Yoo, Terascale direct numerical simulations of turbulent combustion using S3D. Comput. Sci. Discov., 2 (2009) 015001.
[22] S.R. Turns, An introduction to combustion: concepts and applications, 3rd Edition, McGraw Hill (2011).
[23] N. Peters, P. Terhoeven, J.H. Chen, T. Echekki, Statistics of Flame Displacement Speeds from Computations of 2-D Unsteady Methane-Air Flames, Proc. Combust. Inst., 27 (1998) 833-839.
[24] T. Echekki, J.H. Chen, Analysis of the contribution of curvature to premixed flame propagation, Combust. Flame, 118 (1999) 308-311.
[25] S.B. Pope, The evolution of surfaces in turbulence, Int J. Engng. Sci., 26 (5) (1998) 445-469.
[26] S.M. Candel, T. J. Poinsot, Flame stretch and the balance equation for the flame area, Combust. Sci. Tech., 70 (1990) 1-15.
[27] K.W. Jenkins, R.S. Cant, DNS of turbulent flame kernels, In C. Liu, L. Sakell and T. Beautner (Eds.), Proc. 2nd AFOSR Conf. on DNS and LES, Kluwer Academic Publishers, (1999) 192-202.
[28] N. Peters, Turbulent Combustion, Cambridge Monograph on Mechanics, Cambridge University Press, Cambridge (2000).
[29] M. Klein, H. Nachtigal, M. Hansinger, M. Pfitzner and N. Chakraborty, Flame Curvature in High Pressure Bunsen Flames, Proceedings of the 10th Mediterranean Combust. Symp. Naples (2017).
[30] A. Soika, F. Dinkelacker, A. Leipertz, Measurement of resolved flame structure with constant Reynolds number, Proc. Combust. Inst., 27 (1998) 785-792.
[31] E.R. Hawkes, J. H. Chen, Direct numerical simulation of hydrogen-enriched lean premixed methane–air flames, Combust. Flame, 138 (2004) 242-258.
[32] F. O'Young, R.W. Bilger, Scalar gradient and related quantities in turbulent premixed flames, Combust. Flame, 109 (1997) 683-700.
[33] Y.-C. Chen, M. S. Monsour, Investigation of flame broadening in the thin reaction zones regime, Proc. Combust. Inst., 27 (1998) 811-818.
[34] Y.-C. Chen, R. W. Bilger, Experimental investigation of three-dimensional fame front structure in premixed turbulent combustion-I: hydrocarbon/air bunsen fames, Combust. Flame, 131 (2002) 400-435.
[35] N. Chakraborty and S. Cant, Unsteady effects of strain rate and curvature on turbulent premixed flames in an inlet-outlet configuration, Combust. Flame, 137 (2004) 129-147.
[36] N. Chakraborty, R.S. Cant, Influence of Lewis Number on curvature effects in turbulent premixed flame propagation in the thin reaction zones regime, Phys. Fluids, 17 (2005) 105105.
[37] N. Chakraborty, M. Klein, R.S. Cant, Stretch rate effects on displacement speed in turbulent premixed flame kernels in the thin reaction zones regime, Proc. Combust. Inst., 31 (2007) 1385-1392.
[38] N. Chakraborty, M. Klein, R.S. Cant, Effects of turbulent Reynolds number on the displacement speed statistics in the thin reaction zones regime turbulent premixed combustion, J. Combust., 2011 (2011) 473679.
[39] E.R. Hawkes, J.H. Chen, Evaluation of models for flame stretch due to curvature in the thin reaction zones regime, Proc. Combust. Inst., 30 (2004) 647-655.
[40] N. Chakraborty, H. Kolla, R. Sankaran, E. R. Hawkes, J. H. Chen, N. Swaminathan, Determination of three-dimensional quantities related to scalar dissipation rate and its transport from two-dimensional measurements: Direct Numerical Simulation based validation, Proc. Combust. Inst., 34 (2013)1151-1162.